An Optimized Isolation Network for the Wilkinson Divider

Vahdettin Tas, *Student Member, IEEE*, and Abdullah Atalar, *Fellow, IEEE*

***Abstract*—We propose an isolation network to simultaneously improve the input return loss, output return loss and isolation of the Wilkinson power divider in a wide bandwidth. The required even mode and odd mode reflection coefficients of the isolation network are calculated. Constructed even and odd mode circuits are combined to give the desired isolation network. Analytical expressions for the optimal component values for a single-section divider are given. Compared with the single-section Wilkinson divider, the final design can triple the bandwidth for an input-output return loss and isolation of greater than 25 dB. Broadband characteristic is achieved without increasing the number of sections hence extra length and insertion loss are avoided. Wide operation bandwidth of the new divider is verified by experimental results. The proposed method can be applied to a two-section divider, also broadening its bandwidth.**

***Index Terms*—Even mode, isolation network, odd mode, reflection coefficients, wideband power divider, Wilkinson divider.**

I. Introduction

POWER dividers are used at microwave frequencies to direct the power to two or more loads. Normally, they maintain the matched condition at all ports within the operation band. Moreover, a good isolation between the output ports is desired to eliminate the interaction between the loads. When used in the opposite direction, power dividers can combine power from two or more power sources. The Wilkinson power divider was introduced in 1960 [1]. Around the center frequency it is matched at all ports and isolated at the output ports within a relatively narrow bandwidth. Cohn [2] introduced the multisection hybrids to improve the operation bandwidth of the Wilkinson divider. Broadband power division using multisection structures was revealed in several studies [3]–[8]. Wide operation bandwidth is also achieved by utilizing tapered lines. They are constructed using a continuum of a long tapered line [9] or multisection tapered lines [10]. The main disadvantage of using multi sections is the increase in the length and the insertion loss of the divider. To avoid this, a number of researchers designed reduced size dividers [11]–[14]. Another approach to improve the bandwidth response of the Wilkinson divider aims dual band operation. This is achieved by using RLC networks in series or parallel configuration between the output ports [15]–[17], coupled lines [18], parallel stubs along the transmission path [19] and right-left handed transmission lines [20]. These designs also require an increase in length. Other works [21], [22] focus on the isolation network design for isolation bandwidth improvement. Length increment is avoided by modifying only the isolation network. In these works, the isolation bandwidth is widened while the input return loss is kept unchanged. Due to the position of the isolation resistors extra insertion loss is faced.

Our goal is to design an isolation network that improves the bandwidth of input return loss, output return loss and isolation, simultaneously. This way, the number of sections is not increased hence extra length and loss are avoided. We first derive an equation relating the input return loss, output return loss and isolation values of a symmetrical two way power divider. Then we calculate the optimal reflection coefficients of the isolation network in the even mode and odd mode cases. Circuits are constructed to realize the calculated reflection coefficients. The resulting circuits are combined in the final divider structure. Preliminary experimental results of the single-section divider were presented in [23]. Here, detailed analytical work and simulation results for the single and two-section dividers are presented along with new experimental results.

II. S-Parameter Relation for A Lossless Symmetrical 2-Way Divider

In Fig. 1, a symmetrical multisection 2-way combiner/divider network is depicted. The network is composed of lossless lumped or distributed components apart from the isolation arms shown with gray boxes. The contents of the gray boxes are delineated in Fig. 2. It is composed of symmetrical white boxes with resistors in the middle. The white boxes in Figs. 1 and 2 can have more than one series or shunt lossless components as long as the symmetry between the arms is maintained. S-parameter matrix equation of such a three port is given by

$$\begin{bmatrix} b_1 \\ b_2 \\ b_3 \end{bmatrix} = \begin{bmatrix} S_{11} & S_{21} & S_{21} \\ S_{21} & S_{22} & S_{32} \\ S_{21} & S_{32} & S_{22} \end{bmatrix} \begin{bmatrix} a_1 \\ a_2 \\ a_3 \end{bmatrix} \tag{1}$$

where $|a_n|^2$ and $|b_n|^2$ are the incident and reflected powers at port n. $|S_{21}|$ can be expressed as

$$|S_{21}| = \sqrt{\frac{1-|S_{11}|^2}{2}}. \tag{2}$$

If $a_1 = 0$ and $a_2 = a_3 = 1/\sqrt{2}$ are applied, we find

$$|b_1| = \sqrt{1-|S_{11}|^2} \tag{3}$$

Manuscript received June 30, 2014; revised September 22, 2014; accepted October 23, 2014. Date of publication November 14, 2014; date of current version December 02, 2014. This paper is an expanded version from the IEEE MTT-S International Microwave Symposium, Tampa Bay, FL, USA, June 1-6 2014.

The authors are with the Department of Electrical and Electronics Engineering, Bilkent University, Ankara 06800, Turkey (e-mail: vtas@ee.bilkent.edu.tr; aatalar@bilkent.edu.tr).

Color versions of one or more of the figures in this paper are available online at http://ieeexplore.ieee.org.

Digital Object Identifier 10.1109/TMTT.2014.2365533

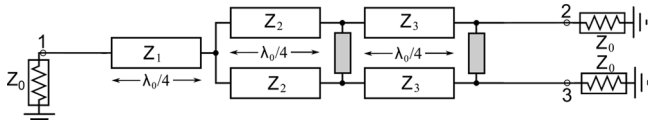

Fig. 1. Symmetrical 2-way power combiner/divider network. White boxes are lossless. Gray boxes represent the lossy isolation arms.

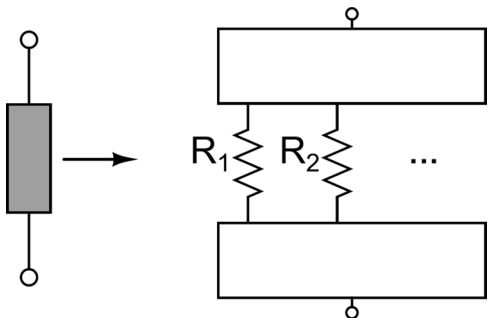

Fig. 2. Possible contents of a gray box: Symmetrical lossless white boxes with isolation resistors in the middle.

$$b_2 = b_3 = \frac{S_{22} + S_{32}}{\sqrt{2}}. \tag{4}$$

The incident power is $|a_2|^2 + |a_3|^2 = 1$. Due to the even excitation, there is no dissipation in the isolation arms, and the total incident power equals the transmitted power plus the total reflected power:

$$|a_2|^2 + |a_3|^2 = |b_1|^2 + |b_2|^2 + |b_3|^2. \tag{5}$$

From (3)–(5) we find

$$1 = |b_1|^2 + |b_2|^2 + |b_3|^2 = (1 - |S_{11}|^2) + |S_{22} + S_{32}|^2 \tag{6}$$

and finally we arrive at the result[1]

$$|S_{11}| = |S_{22} + S_{32}|. \tag{7}$$

Corollary 1: For the generic 2-way divider of Fig. 1, if $|S_{22} + S_{32}| < \delta$ and $|S_{22} - S_{32}| < \delta$, then $|S_{11}| < \delta$, $|S_{22}| < \delta$ and $|S_{32}| < \delta$.

Proof: Defining $S_{22} + S_{32} = \delta_1 e^{j\theta_1}$ and $S_{22} - S_{32} = \delta_2 e^{j\theta_2}$, where $\delta_1, \delta_2 \leq \delta$ and θ_1, θ_2 are arbitrary angles, we have

$$|S_{22}| = \frac{|\delta_1 e^{j\theta_1} + \delta_2 e^{j\theta_2}|}{2} \leq \frac{(\delta_1 + \delta_2)}{2} \leq \delta \tag{8}$$

$$|S_{32}| = \frac{|\delta_1 e^{j\theta_1} - \delta_2 e^{j\theta_2}|}{2} \leq \frac{(\delta_1 + \delta_2)}{2} \leq \delta. \tag{9}$$

$|S_{11}| < \delta$ directly follows from (7).

For the generalized two-way divider in Fig. 1, the excitation $a_1 = 0, a_2 = 1, a_3 = 1$ results in the even mode operation. The S-parameter matrix (1) can be rewritten as

$$\begin{bmatrix} b_1 \\ b_2 \\ b_3 \end{bmatrix} = \begin{bmatrix} S_{11} & S_{21} & S_{21} \\ S_{21} & S_{22} & S_{32} \\ S_{21} & S_{32} & S_{22} \end{bmatrix} \begin{bmatrix} 0 \\ 1 \\ 1 \end{bmatrix}. \tag{10}$$

[1]Equation (7) was implicitly stated in [2].

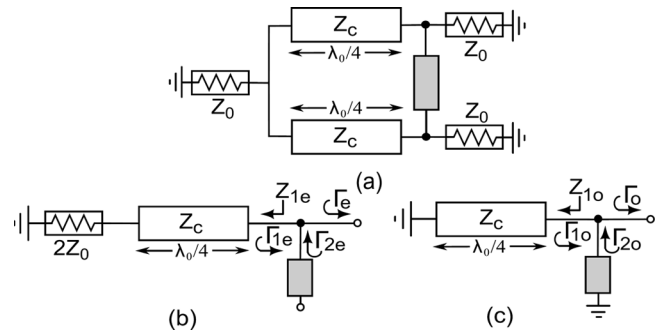

Fig. 3. (a) Single-section Wilkinson divider with a gray box in the isolation arm. (b) Even mode equivalent circuit. c) Odd mode equivalent circuit.

So, the reflection coefficient at the second port equals to

$$\Gamma_e = \frac{b_2}{a_2} = S_{22} + S_{32}. \tag{11}$$

Similarly, the excitation $a_1 = 0$, $a_2 = 1$, $a_3 = -1$ results in the odd mode operation. The S-parameter matrix (1) can be rewritten as

$$\begin{bmatrix} b_1 \\ b_2 \\ b_3 \end{bmatrix} = \begin{bmatrix} S_{11} & S_{21} & S_{21} \\ S_{21} & S_{22} & S_{32} \\ S_{21} & S_{32} & S_{22} \end{bmatrix} \begin{bmatrix} 0 \\ 1 \\ -1 \end{bmatrix}. \tag{12}$$

So, the reflection coefficient at the second port equals to

$$\Gamma_o = \frac{b_2}{a_2} = S_{22} - S_{32}. \tag{13}$$

$S_{22} + S_{32}$ and $S_{22} - S_{32}$ are the even mode (Γ_e) and odd mode (Γ_o) reflection coefficients at port 2. From Corollary 1 we can conclude that keeping the even mode and odd mode reflection coefficients at port 2 below a certain level assures that the input-output return loss and isolation parameters are kept below the same level.

In the literature, broadband operation of the power dividers is generally achieved at the expense of an increase in the length and insertion loss of the dividers. In those designs, the isolation networks are composed of floating components without a ground connection, hence the isolation network does not affect the even mode circuit. Consequently, the input return loss can not be tuned by the isolation network. This is a significant loss of a degree of freedom. By the inclusion of components with a ground connection, the isolation network can be active both in the even mode as well as in the odd mode. With such an approach both $S_{22} - S_{32}$ and $S_{22} + S_{32}$ can be tuned by the isolation network.

III. Optimal Choice of Isolation Network in the Even and Odd Modes

Our goal is to find an optimal isolation network for the single-section Wilkinson divider depicted in Fig. 3(a). The isolation network is represented with a gray box. Z_c can be different than $\sqrt{2}Z_0$ for generality. Fig. 3(b) and (c) shows the even and odd mode equivalent circuits with the gray box open-circuited and shorted at its mid point, respectively.

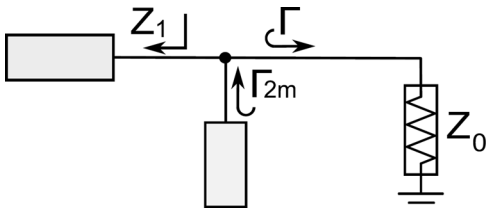

Fig. 4. Two networks connected in parallel. One has an input impedance of Z_1, the other one has an input reflection coefficient of Γ_{2m} to give $\Gamma = 0$.

For a parallel connection of two one-port networks shown in Fig. 4, the perfect match condition ($\Gamma = 0$) requires

$$\Gamma_{2m} = \frac{1}{2\overline{Z}_1 - 1} \quad \text{for} \quad \overline{Z}_1 \neq 0 \tag{14}$$

where $\overline{Z}_1 = Z_1/Z_0$ is the normalized input impedance of the first block and Γ_{2m} is the input reflection coefficient of the second block giving the perfect match.

The normalized impedances $\overline{Z}_{1e}$ and $\overline{Z}_{1o}$ defined in Fig. 3 are equal to

$$\overline{Z}_{1e} = \frac{Z_{1e}}{Z_0} = \frac{2 + j\overline{Z}_c \tan(\frac{\pi f}{2f_0})}{1 + j\frac{2}{\overline{Z}_c}\tan(\frac{\pi f}{2f_0})} \tag{15}$$

$$\overline{Z}_{1o} = \frac{Z_{1o}}{Z_0} = j\overline{Z}_c \tan(\frac{\pi f}{2f_0}) \tag{16}$$

where f_0 ($= w_0/2\pi$) is the center frequency and $\overline{Z}_c = Z_c/Z_0$. The reflection coefficients Γ_{2em} and Γ_{2om} of the even and odd mode isolation circuits that will generate a perfect match can be calculated using (14), (15), and (16):

$$\Gamma_{2em} = \frac{1 + j\frac{2}{\overline{Z}_c}\tan(\frac{\pi f}{2f_0})}{3 + j(2\overline{Z}_c - \frac{2}{\overline{Z}_c})\tan(\frac{\pi f}{2f_0})} \tag{17}$$

$$\Gamma_{2om} = \frac{1}{j2\overline{Z}_c \tan(\frac{\pi f}{2f_0}) - 1}. \tag{18}$$

A. Even Mode Isolation Circuit

The trajectory of Γ_{2em} is drawn on the Smith chart of Fig. 5 for $\overline{Z}_c = 0.95\sqrt{2}$, $\sqrt{2}$ and $1.05\sqrt{2}$. Even mode isolation circuit must be lossless, otherwise the insertion loss of the divider will increase. So, its reflection coefficient must lie on the unity circle of the Smith chart. Γ_{2em} characteristic can be approximated with a shorted quarter-wave stub of impedance Z_p as in Fig. 6. The corresponding Γ_{2e} is depicted by dashed lines in Fig. 5. For $\overline{Z}_c = \sqrt{2}$, Γ_{2e} and Γ_{2em} coincide only at the center frequency and deviate fast with frequency. For $\overline{Z}_c > \sqrt{2}$, the situation is even worse. With $\overline{Z}_c < \sqrt{2}$, Γ_{2e}, and Γ_{2em} coincide at two frequencies and the highest deviation occurs at the center frequency, f_0, and at band edges. This characteristic resembles a second degree Chebyshev response maximizing the bandwidth. So, we choose $\overline{Z}_c < \sqrt{2}$ to have a wideband approximation. The deviation at f_0 can be adjusted by the value of Z_c. At f_0, the shorted quarter-wave stub (Z_p) acts like an open-circuit. Using Corollary-1 we aim to satisfy $|\Gamma_e| \leq \delta$. The deviation is maximum at f_0, so $|\Gamma_e(f_0)| = \delta$. Referring to Fig. 6, since $\Gamma_e = \Gamma_{1e}$ at f_0, the value of $Z_{1e}(f_0)$ is equal to

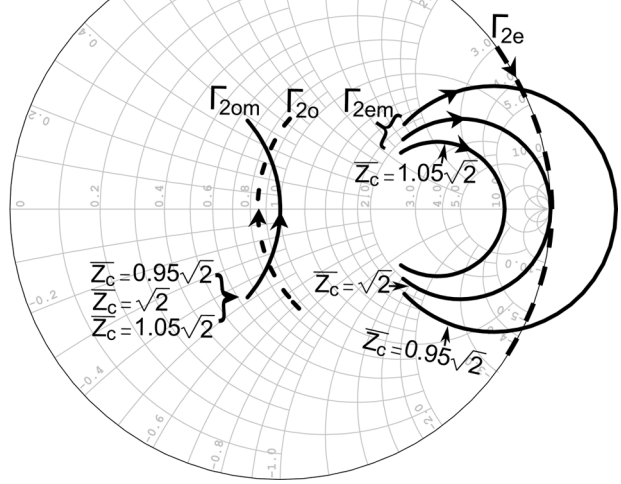

Fig. 5. Γ_{2em} and Γ_{2om} on the Smith chart (solid lines) as the frequency is swept from $f_0/2$ to $3f_0/2$ (in the direction of arrows) for $\overline{Z}_c = 0.95\sqrt{2}$, $\sqrt{2}$ and $1.05\sqrt{2}$. Approximations, Γ_{2e} and Γ_{2o}, (dashed lines) are also shown.

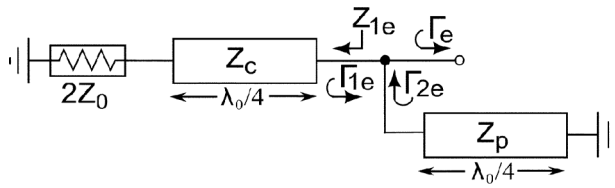

Fig. 6. Even mode equivalent circuit with the shorted quarter-wave stub of impedance Z_p at the isolation arm.

$$Z_{1e}(f_0) = \frac{Z_c^2}{2Z_0} = Z_0\frac{1-\delta}{1+\delta}. \tag{19}$$

Hence, we have

$$\overline{Z}_c = \sqrt{\frac{2(1-\delta)}{1+\delta}} \approx \sqrt{2}(1-\delta). \tag{20}$$

To calculate the bandwidth and the optimal value of Z_p, we refer to the Smith chart shown in Fig. 7. The goal is to bend the Z_{1e} trajectory into the $|\Gamma_e| = \delta$ circle using the shorted transmission line with the characteristic impedance of Z_p. The lowest normalized conductance on the locus of the $|\Gamma_e| = \delta$ circle is $(1-\delta)/(1+\delta)$. So, the frequencies at which Z_{1e} results a conductance of $(1-\delta)/(1+\delta)$ are the minimum and the maximum frequencies satisfying the $|\Gamma_e| \leq \delta$ condition. The lower and upper frequencies are marked as f_1 and f_2, respectively, in Fig. 7.

At $f = f_1$, we have:

$$Re\left\{\frac{1}{\overline{Z}_{1e}(f_1)}\right\} = \frac{1-\delta}{1+\delta}. \tag{21}$$

Using (15) and (20), (21) can be expanded as

$$Re\left\{\frac{\sqrt{2}(1-\delta) + j2\tan(\frac{\pi f_1}{2f_0})}{2(1-\delta)[\sqrt{2} + j(1-\delta)\tan(\frac{\pi f_1}{2f_0})]}\right\} = \frac{1-\delta}{1+\delta}. \tag{22}$$

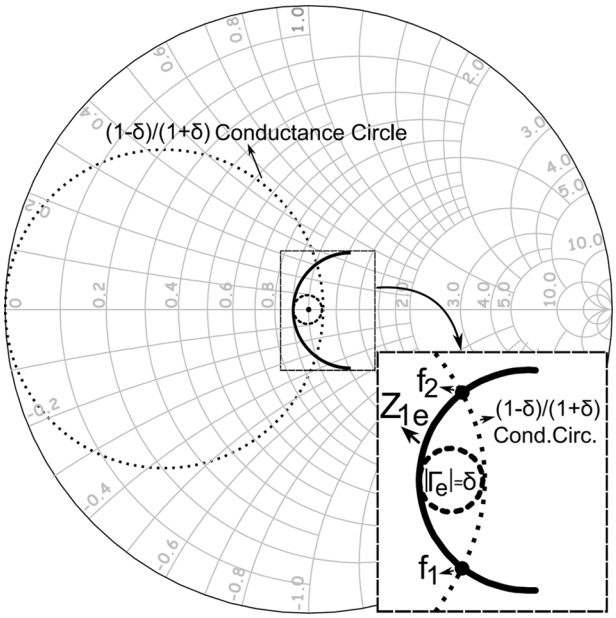

Fig. 7. Trajectories of the $(1-\delta)/(1+\delta)$ constant conductance circle and $|\Gamma_e| = \delta$ circle along with the trajectory of Z_{1e} (shown in Fig. 6).

We find

$$\tan(\frac{\pi f_1}{2f_0}) = \sqrt{\frac{1-3\delta}{4\delta - 3\delta^2 + \delta^3}}. \tag{23}$$

For small δ, we can ignore the δ^3 term, and write f_1 as

$$\frac{f_1}{f_0} \approx \frac{2}{\pi}\tan^{-1}\sqrt{\frac{1-3\delta}{4\delta - 3\delta^2}}. \tag{24}$$

We note that $f_2 - f_0 = f_0 - f_1$. For example, for $\delta = 0.1(-20\text{ dB})$, $f_1 = 0.6f_0$ and $f_2 = 1.4f_0$.

The value of Z_p is calculated by considering that the imaginary part of the $1/Z_{1e}$ admittance should be compensated perfectly at f_1:

$$Im\left\{\frac{1}{\overline{Z}_{1e}}\right\} = \frac{1}{\overline{Z}_p \tan(\frac{\pi f_1}{2f_0})}. \tag{25}$$

So, we have

$$Im\left\{\frac{\sqrt{2}(1-\delta) + j2\tan(\frac{\pi f_1}{2f_0})}{2(1-\delta)[\sqrt{2} + j(1-\delta)\tan(\frac{\pi f_1}{2f_0})]}\right\} = \frac{1}{\overline{Z}_p \tan(\frac{\pi f_1}{2f_0})}. \tag{26}$$

Using (24) the value of $\overline{Z}_p$ is extracted from (26) as

$$\overline{Z}_p \approx \sqrt{2}\frac{1+2\delta-2\delta^2}{1-\delta-7\delta^2}. \tag{27}$$

$\overline{Z}_p$ approaches to $\sqrt{2}$ as δ gets closer to zero. With $\delta = 0.1$, (27) results in $\overline{Z}_p = 2.0$

If a lumped circuit is preferred, this shorted $\lambda/4$ line can be approximated as a parallel LC circuit [24] with the component values expressed as

$$w_0 L_p = \frac{4Z_p}{\pi} \quad \text{and} \quad L_p C_p = \frac{1}{w_0^2}. \tag{28}$$

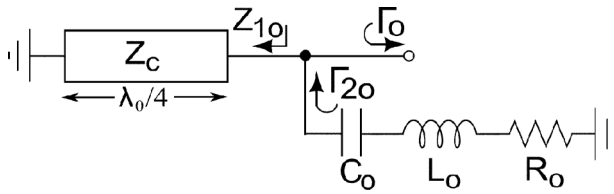

Fig. 8. Odd mode equivalent circuit with the optimal isolation network. L_o and C_o are resonant at the center frequency f_0.

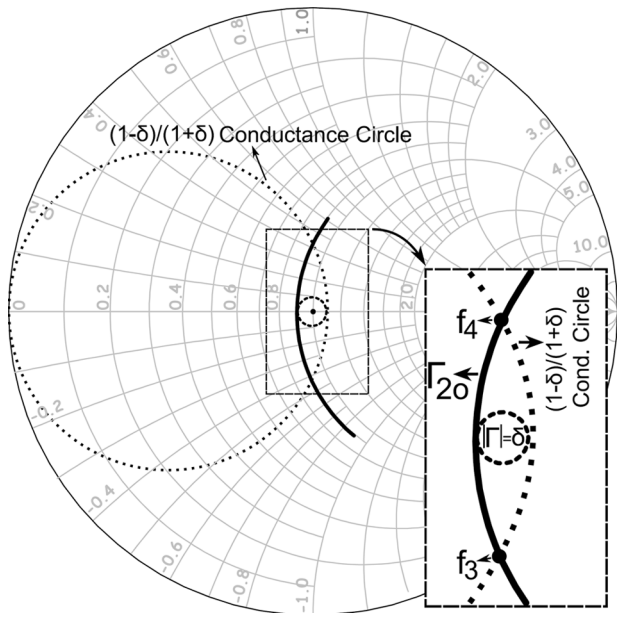

Fig. 9. Trajectories of the $(1-\delta)/(1+\delta)$ constant conductance circle and $|\Gamma| = \delta$ circle along with the trajectory of Γ_{2o} of Fig. 8.

B. Odd Mode Isolation Circuit

Smith chart trajectories of Γ_{2om} for three different Z_c values (which are almost equal to each other) are shown in Fig. 5. The locus of Γ_{2om} follows a constant conductance circle. A series RLC circuit resonant at f_0 shown in Fig. 8 can be utilized to approximate the desired characteristics.

The same approach as the even mode case is followed to calculate the component values of the odd mode isolation network analytically. Referring to Fig. 8, Γ_{2o} is the reflection coefficient of the series $R_o L_o C_o$ network. The goal is to maximize the bandwidth of the $|\Gamma_o| \leq \delta$ condition. Fig. 9 shows the $|\Gamma| = \delta$ circle on the Smith chart together with the trajectory of Γ_{2o}. The points marked as f_3 and f_4 represent the edge frequencies that Γ_{2o} can be fitted into the $\Gamma = \delta$ circle by the shorted stub of impedance Z_c.

The impedance of a series LC resonator is not symmetric around the center frequency. We have $f_4 - f_0 > f_0 - f_3$. Therefore, $2(f_0 - f_3)$ is the bandwidth of the $|\Gamma_o| \leq \delta$ condition. For the circuit in Fig. 8 at f_0, C_o resonates with L_o and the quarter-wave stub Z_c is open-circuit. We have $\Gamma_o(f_0) = \Gamma_{2o}(f_0) = (R_o - Z_0)/(R_o + Z_0)$. As shown in Fig. 9, $\Gamma_{2o}(f_0) = -\delta$. So, the value of the resistor is equal to

$$\overline{R}_o = \frac{R_o}{Z_0} = \frac{1-\delta}{1+\delta}. \tag{29}$$

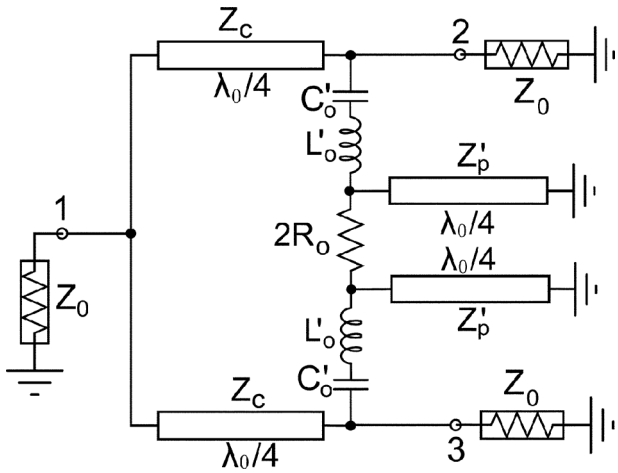

Fig. 10. Schematic diagram of the divider by merging the optimal even mode and odd mode isolation networks.

L_o can be calculated by imposing two conditions at $f = f_3$. Γ_{2o} trajectory crosses the $(1-\delta)/(1+\delta)$ conductance circle and the transmission line with the impedance of Z_c compensates the reactive part of Γ_{2o} perfectly. So, we have two equations:

$$Re\left\{\frac{Z_0}{R_o - j2\pi f_3 L_o\left(\frac{f_0^2}{f_3^2}-1\right)}\right\} = \frac{1-\delta}{1+\delta} \tag{30}$$

$$Im\left\{\frac{Z_0}{R_o - j2\pi f_3 L_o\left(\frac{f_0^2}{f_3^2}-1\right)}\right\} = \frac{1}{Z_c \tan(\frac{\pi f_3}{2f_0})}. \tag{31}$$

Using (29) and (30) we find

$$2\pi f_3 \frac{L_o}{Z_0}\left(\frac{f_0^2}{f_3^2}-1\right) = \frac{2\sqrt{\delta}}{1+\delta}. \tag{32}$$

Inserting (32) in the denominator of (31) and using (20), f_3 is calculated as

$$\frac{f_3}{f_0} = \frac{2}{\pi}\tan^{-1}\left(\frac{(1+\delta)^{3/2}}{\sqrt{8\delta(1-\delta)}}\right). \tag{33}$$

Equation (33) together with (32) result in

$$\frac{w_0 L_o}{Z_0} = \frac{2\sqrt{\delta}}{1+\delta}\frac{\frac{f_0}{f_3}}{\left(\frac{f_0}{f_3}\right)^2 - 1}. \tag{34}$$

For example, with $Z_0 = 50\Omega$ and $\delta = 0.1$, we find $f_3 = 0.596 f_0$ and $L_o = 4.23$ nH. We note that the odd mode bandwidth is greater than the even mode bandwidth.

IV. Combining the Even and Odd Mode Isolation Networks

We merge the isolation circuits of Figs. 6 and 8 as shown in Fig. 10. Fig. 11 depicts the approximations involved in the merging process. Due to the interaction between the even and odd mode networks, some component values are shown with a prime symbol to indicate a possible modification in the calculated component values of the previous section.

The value of Z_c was determined in the even mode circuit by the condition at f_0. Since the isolation network does not affect

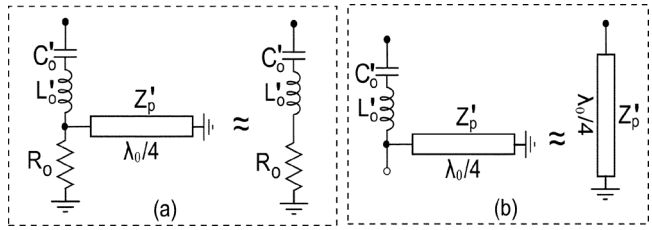

Fig. 11. Equivalent representation of the isolation network for the divider in Fig. 10. (a) Odd-mode. (b) Even-mode.

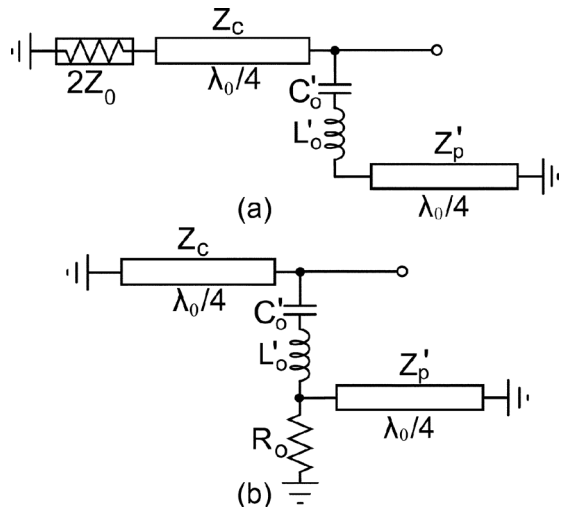

Fig. 12. Even (upper) and odd (lower) mode equivalent circuits of the divider in Fig. 10.

the even mode circuit at f_0, Z_c value of (20) will not be modified. Similarly, R_o was determined in the odd mode circuit by the condition at f_0. Since $Z_p{}'$ is open circuit at f_0, the value of R_0 given in (29) will not change.

The new values of $Z_p{}'$ and $L_0{}'$ can be calculated following the analysis of the previous sections. Fig. 12 shows the even and odd mode equivalent circuits of the divider. Referring to Fig. 12(a), (26) is modified due to the presence of $L_o{}'$ and $C_o{}'$:

$$Im\left\{\frac{\sqrt{2}(1-\delta)+j2\tan(\frac{\pi f_1}{2f_0})}{2(1-\delta)[\sqrt{2}+j(1-\delta)\tan(\frac{\pi f_1}{2f_0})]}\right\} = \\ = \frac{Z_0}{Z'_P\tan(\frac{\pi f_1}{2f_0}) - 2\pi f_1 L'_o\left(\frac{f_0^2}{f_1^2}-1\right)} \tag{35}$$

where f_1 is expressed in (24). f_1 is independent of the problem handled here, it is determined solely by Z_c.

From Fig. 12(b), (30) and (31) are modified to

$$Re\left\{\frac{Z_0}{R_o \| jZ'_p\tan(\frac{\pi f'_3}{2f_0}) - j2\pi f'_3 L'_o\left(\frac{f_0^2}{f_3'^2}-1\right)}\right\} = \frac{1-\delta}{1+\delta} \tag{36}$$

$$Im\left\{\frac{Z_0}{R_o | jZ'_p\tan(\frac{\pi f'_3}{2f_0}) - j2\pi f'_3 L'_o\left(\frac{f_0^2}{f_3'^2}-1\right)}\right\} = \frac{Z_0}{Z_c\tan(\frac{\pi f'_3}{2f_0})}. \tag{37}$$

f'_3 is used instead of the f_3 in (33) because it is dependent on Z'_p and L'_o. A simultaneous solution of (35), (36), and (37) to find f'_3, Z'_p and L'_o is not possible. To find the values, the mean square

TABLE I
NORMALIZED COMPONENT VALUES FOR INPUT–OUTPUT RETURN LOSSES AND ISOLATION BETTER THAN δ (dB).

δ (dB)	$\Delta f/f_0$	$\overline{Z}_c$	$2\overline{R}_o$	$\overline{w_0 L_o}'$	$\overline{Z}_p'$
-20	0.80	1.28	1.63	0.64	2.41
-25	0.60	1.34	1.79	0.84	1.98
-30	0.45	1.37	1.88	0.96	1.73
-35	0.34	1.39	1.93	1.02	1.59
-40	0.25	1.4	1.96	1.06	1.51

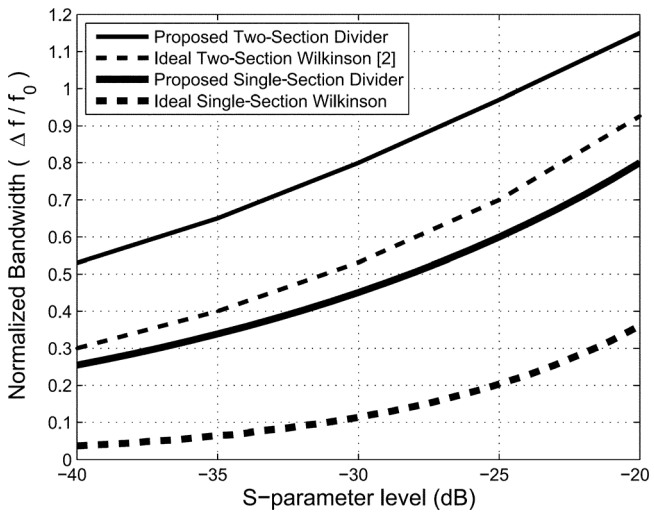

Fig. 13. Normalized bandwidth comparison of the prosed divider structure with the classical single-section Wilkinson divider and Cohn's design of two-section Wilkinson divider [2].

error in these equations are minimized numerically. Results of the numerical calculations are used to express Z_p' and L_o' by the following approximations

$$\overline{Z}_p' = \frac{Z_p'}{Z_0} \approx \sqrt{2} + 10\delta \tag{38}$$

$$\overline{w_0 L_o}' = \frac{w_0 L_o'}{Z_0} \approx 1.1 - 4.6\delta. \tag{39}$$

Table I lists the results normalized with Z_0. The achievable normalized bandwidth and required component values for the corresponding δ level are listed. The divider bandwidth, Δf, is limited by the bandwidth of the even mode circuit: $\Delta f = 2(f_0 - f_1)$. Z_c, f_1, R_o, Z_p', and L_o' are determined from (20), (24), (29), (38), and (39), respectively. C_o' is resonant with L_o' at f_0. Our results are verified using a microwave circuit simulator.[2]

It is possible to apply the proposed method to a two-section divider. Using a similar isolation arm for both sections, it is possible to extend the bandwidth considerably. The results for the two-section case are given in Appendix A.

Fig. 13 compares the bandwidth capabilities of the proposed single-section and two-section dividers with the classical single-section Wilkinson divider and Cohn's two-section Wilkinson divider [2]. A significant bandwidth improvement is achieved. For 25 dB of input–output return loss and isolation, three times wider bandwidth is obtained in comparison to a single-section Wilkinson. The bandwidth of a two-section Wilkinson divider is almost reached with a single-section divider, avoiding the extra size and insertion loss of the two-section divider.

[2]AWR Corp. El Segundo, CA 90245, USA, http://www.awrcorp.com

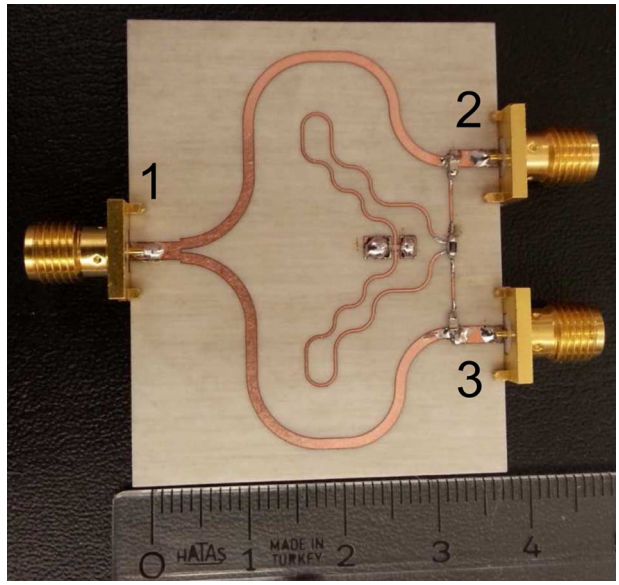

Fig. 14. Implemented 2-way power divider of Fig. 10.

In terms of insertion loss, the proposed divider is similar to a single-section Wilkinson divider, because the input signal propagates a distance of exactly one quarter wavelength. In fact, our divider is more advantageous in terms of the loss, since the impedance transforming line has a characteristic impedance smaller than $\sqrt{2}Z_0$ resulting in a wider line width. Considering the size of the divider, the $\lambda_0/4$ line in the isolation arm is shorted at one end and it has a high characteristic impedance with a narrow width. This enables one to use layout techniques such as bending or meandering of the line to get a compact size. We note that a two-section Wilkinson divider with two isolation resistors cannot be shaped in the same manner to reduce the size.

We note that presence of a ground path in the isolation network generates nulls in S_{21}. These frequencies can be calculated by considering the sum of the impedances of the Z_p' line and $L_o'C_o'$ pair:

$$Z_p' \tan(\frac{\pi f}{2f_0}) - 2\pi f L_o' \left(\frac{f_0^2}{f^2} - 1\right) = 0. \tag{40}$$

Using (38) and (39), (40) can be rewritten as

$$(\sqrt{2} + 10\delta)\tan(\frac{\pi f}{2f_0}) = (1.1 - 4.6\delta)\frac{f}{f_0}\left(\frac{f_0^2}{f^2} - 1\right). \tag{41}$$

For example, for $\delta = 0.1$ $(-20$ dB), (41) is satisfied at two frequencies, at $0.36f_0$ and $1.8f_0$, outside the operation bandwidth $(0.6f_0 - 1.4f_0)$ of the divider.

V. SIMULATION AND EXPERIMENTAL RESULTS

The proposed divider in Fig. 10 is implemented for experimental verification at a center frequency of $f_0 = 1$ GHz. $\delta =$

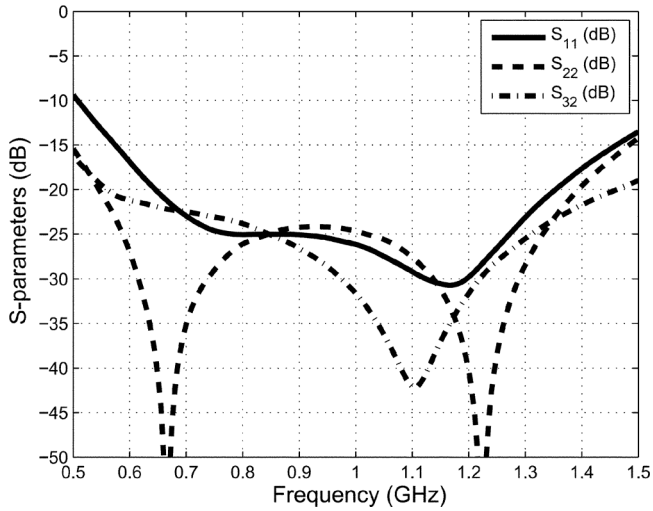

Fig. 15. Simulated S-parameter characteristics of the divider in Fig. 14.

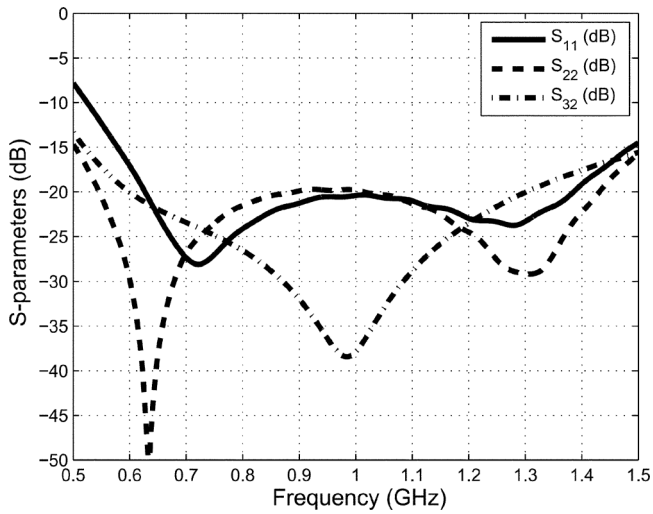

Fig. 16. Measured S-parameter characteristics of the divider in Fig. 14.

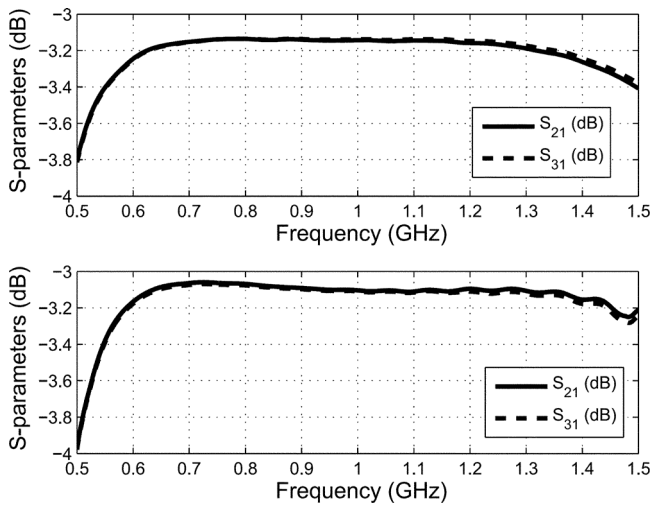

Fig. 17. Simulated (upper) and measured (lower) S-parameter characteristics of the divider in Fig. 14.

-20 dB is the design goal. As shown in Table I, the theoretical fractional bandwidth is $\Delta f/f_0 = 0.8$ implying a 20-dB bandwidth of 0.6 GHz to 1.4 GHz. The divider is simulated using

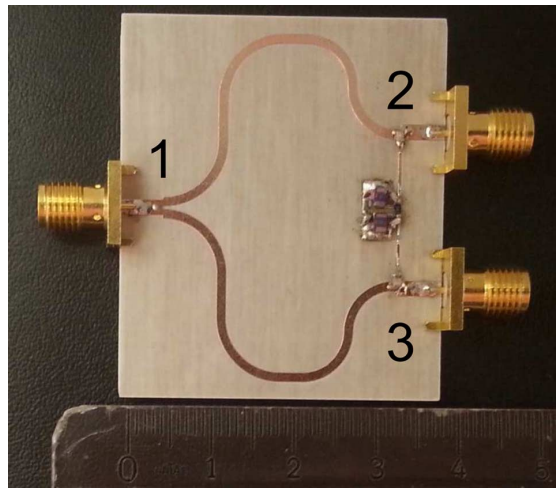

Fig. 18. Modified version of divider in Fig. 14 upon the replacement of the shorted $\lambda_0/4$ lines with the parallel LC resonators.

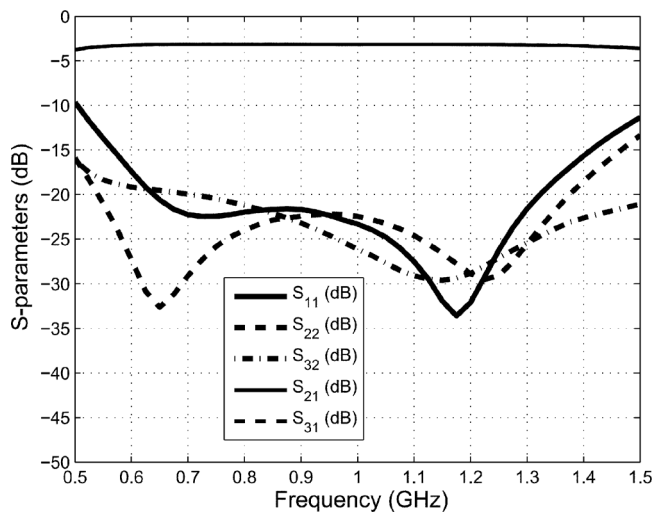

Fig. 19. Simulated response of the divider in Fig. 18.

the microwave circuit simulator and an electromagnetic simulator.[3] With ideal components, $\Delta f/f_0 = 0.8$ is achieved using the values given in Table I. Inclusion of the junction effects and component parasitics result in a reduction of the bandwidth. To alleviate these effects, the component values are tuned slightly.

Fig. 14 shows the photo of the divider implemented on a RO4003[4] substrate with a thickness of 0.8 mm. L_o inductors are implemented using high impedance microstrip lines of 0.3 mm in width and 6.7 mm in length. Presence of L_o in the isolation circuit provides a natural separation between ports 2 and 3, reducing the length of subsequent connections and improving the isolation between the output ports [25], [26]. In the divider of Fig. 14, the width of Z_c lines are 1.1 mm corresponding to a characteristic impedance of 66 Ω. Z_p lines have a width of 0.3 mm resulting in an impedance of 116 Ω. 0603 package 5.6-pF capacitors and a 75 Ω resistor are used. Figs. 15 and 17 show the simulation results of the electromagnetic simulator. The output return loss and the isolation are better than 20 dB in the targeted

[3]SONNET Software, North Syracuse NY 13212, USA, http://www.sonnet-software.com

[4]Rogers Corp. Rogers, CT 06263, USA, http://www.rogerscorp.com

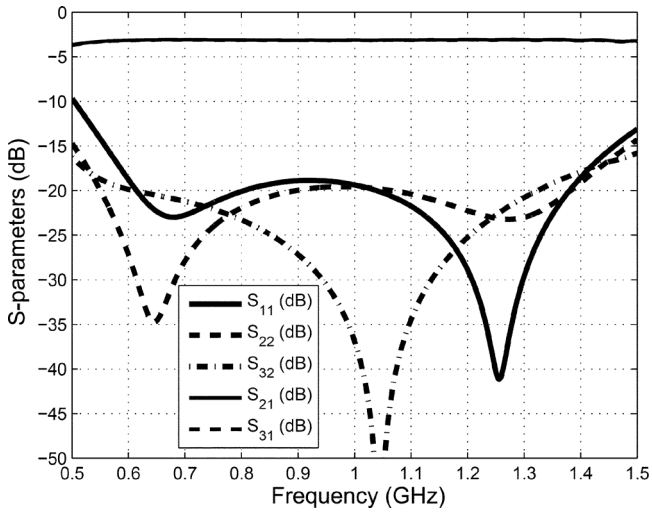

Fig. 20. Measured response of the divider in Fig. 18.

TABLE II
COMPARISON TABLE

Reference	Technique	Size	Normalized Bandwidth	Loss (dB)
[5]	Microcoaxial Multisection	$6\lambda_0/4$	20-dB: 1.10	1
[27]	Multi Wafer Multisection	λ_0	15-dB: 1.15	1
[10]	Tapered Multisection	$5\lambda_0/6$	15-dB: 1.60	0.3
[7]	Three-section Coplanar Waveguide	$3\lambda_0/4$	15-dB: 1.15	0.8
[12]	Lumped Inductors	$\lambda_0/10$	20-dB: 0.15	0.3
[28]	Right-Left Handed isolation elements	$\lambda_0/4$	20-dB: 0.38	0.3
[29]	Single-section Trantanella	$\lambda_0/4$	20-dB: 0.36	0.2
[30]	Single-section Complex Termination	$\lambda_0/4$	20-dB: 0.15	0.1
[14]	Complex Isolation Components	$\lambda_0/4$	20-dB: 0.10	0.15
[21]	Single-section Modified Isolation Network	$\lambda_0/4$	18-dB: 0.40	0.5
This Work (Fig. 14)	Single-section Optimized Isolation Network	$\lambda_0/4$	20-dB: 0.68	0.2
This Work (Fig. 18)	Single-section Optimized Isolation Network	$\lambda_0/4$	19-dB: 0.75	0.2

bandwidth, the input return loss drops to 17 dB at the band edges due to the nonideal effects.

Measured input–output return loss, isolation and insertion loss responses are shown in Figs. 16 and 17. The measurement results match the simulation results well. In the operation band, the extra insertion loss is less than 0.2 dB and the amplitude mismatch between the output ports is lower than 0.025 dB.

As discussed in (28) of Section III-A, the shorted $\lambda_0/4$ lines at the isolation arm can be replaced with lumped components. For a verification, a modified version of the divider in Fig. 14 is implemented (Fig. 18). Equation (28) results in $L_p = 23.5$ nH and $C_p = 1.08$pF for 116 Ω characteristic impedance and 1-GHz center frequency. Available chip inductor with a value closest

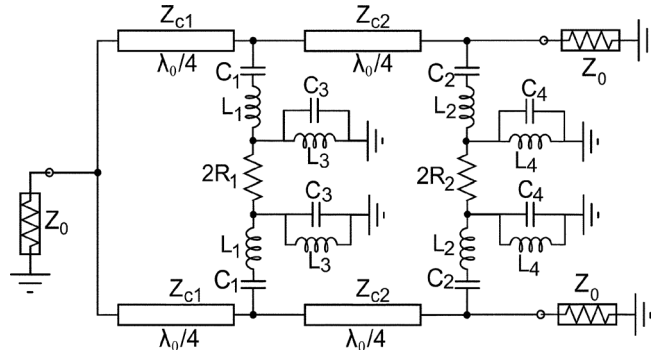

Fig. 21. Two-section divider with the optimal isolation networks.

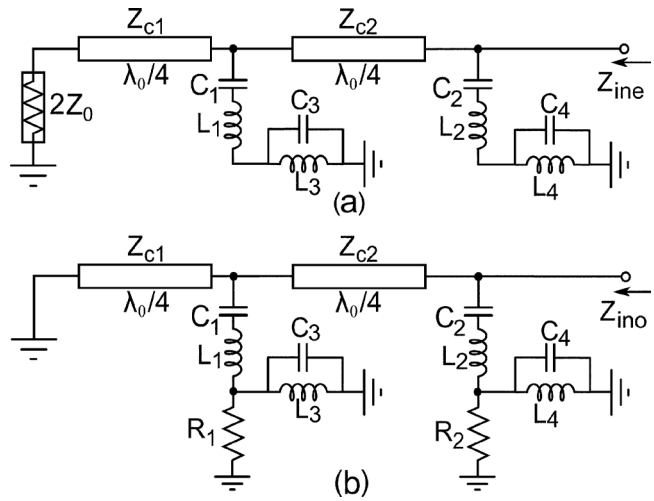

Fig. 22. Even mode (a) and odd mode (b) equivalent circuits of the divider in Fig. 21.

TABLE III
NORMALIZED COMPONENT VALUES FOR INPUT–OUTPUT RETURN LOSSES AND ISOLATION BETTER THAN δ (dB) FOR THE DIVIDER IN FIG. 21

δ	$\overline{\Delta f}$	$\overline{Z}_{c1}$	$\overline{Z}_{c2}$	$\overline{w_0 L_2}$	$\overline{w_0 L_3}$	$\overline{w_0 L_4}$	$2\overline{R}_1$	$2\overline{R}_2$
-20	1.15	1.60	1.25	0.68	–	6.88	1.97	3.36
-25	0.97	1.63	1.22	1.03	–	5.84	1.76	3.76
-30	0.80	1.66	1.21	1.30	26.8	5.30	1.74	4.25
-35	0.65	1.67	1.20	1.53	13	4.94	1.63	4.27
-40	0.53	1.67	1.19	1.65	10	4.77	1.46	3.94

to the calculated one is a 20-nH 0805 package chip inductor. S-parameter data provided by the manufacturer shows that the equivalent inductance of the 20-nH chip inductor increases up to 35 nH at 2 GHz due to the parasitic capacitance. This requires a reduction in the calculated value of C_p. The best performance is obtained using a 0.8-pF capacitor. Figs. 19 and 20 show the simulated and measured results, respectively. The characteristic is similar to the case with the shorted line. 19-dB bandwidth spans the 0.6 GHz to 1.35 GHz frequency range. The insertion loss is again below 0.2 dB in the operation bandwidth.

Table II is a comparison[5] of the dividers of recent studies. Given normalized bandwidth values are valid at the specified

[5]The loss comparison in the table is not totally fair, because the upper frequencies and the substrate materials of the dividers listed in the table are not the same.

dB values of input return loss, output return loss and isolation. Our designs have a wide bandwidth with a low insertion loss and compact size, at the expense of the increased number of components. This increases the circuit implementation complexity and the parasitic problem.

VI. Conclusion

Starting from a fundamental S-parameter relation of a lossless power divider, we find that minimizing the even and odd mode reflection coefficients of an output port is sufficient to optimize a power divider. Using this fact, we are able to synthesize even and odd mode isolation networks to maximize the bandwidth of a single-section Wilkinson divider. The reflection coefficients of the isolation network that perfectly match the even and odd mode circuits are calculated individually. Then, circuits are designed to realize the required reflection coefficients. The even mode and odd mode isolation networks are merged in a configuration to load each other minimally. Analytical expressions are derived for the component values of those networks. A modification in the final component values may be required to alleviate the loading effects. Table I lists the optimal component values.

The resulting divider has a considerably wider operation bandwidth compared to the classical Wilkinson divider. Experimental verification is presented proving that the proposed low-loss divider is promising for wide band applications. The method can be applied to a two-section divider. Using a similar isolation arm for both sections, it is possible to extend the bandwidth considerably.

Appendix
Two-Section Divider With the Optimized Isolation Networks

The optimized isolation network is applied to the two-section case as shown in Fig. 21. The even mode and odd mode equivalent circuits are shown in Fig. 22. Z_{ine} and Z_{ino} represent the input impedances in each mode, respectively.

At f_0, the even mode circuit shown in Fig. 22(a) is composed of only Z_{c1} and Z_{c2}. They provide an impedance transformation from $2Z_0$ to Z_0. The optimal impedance values satisfy the geometric mean condition [31]:

$$Z_{c1}Z_{c2} = 2Z_0^2. \tag{42}$$

By allowing a nonzero reflection coefficient magnitude of δ, the bandwidth of operation can be extended. At the band center, f_0, we have a real reflection coefficient of δ[23]. So, we can write

$$\frac{Z_{c2}^2}{Z_{c1}^2}\frac{2Z_0}{} = Z_0\frac{1+\delta}{1-\delta}. \tag{43}$$

Using (42) and (43), Z_{c1} and Z_{c2} are calculated as

$$\overline{Z}_{c1} = \frac{Z_{c1}}{Z_0} \approx 2^{3/4}(1-\frac{\delta}{2}) \tag{44}$$

$$\overline{Z}_{c2} = \frac{Z_{c2}}{Z_0} \approx 2^{1/4}(1+\frac{\delta}{2}). \tag{45}$$

Even-mode input impedance can be expressed as

$$Z_{ine} = \left(Z_{c2}\frac{Z_x + jZ_{c2}\tan(\frac{\pi f}{2f_0})}{Z_{c2} + jZ_x\tan(\frac{\pi f}{2f_0})}\right) \parallel \left(j2\pi\ fL_2(1-\frac{f_0^2}{f^2}) + \frac{j2\pi fL_4}{1-\frac{f_0^2}{f^2}}\right) \tag{46}$$

where

$$Z_x = \left(Z_{c1}\frac{2Z_0 + jZ_{c1}\tan(\frac{\pi f}{2f_0})}{Z_{c1} + j2Z_0\tan(\frac{\pi f}{2f_0})}\right) \parallel \left(j2\pi fL_1(1-\frac{f_0^2}{f^2}) + \frac{j2\pi fL_3}{1-\frac{f_0^2}{f^2}}\right). \tag{47}$$

The odd mode input impedance can be expressed as

$$Z_{ino} = \left(Z_{c2}\frac{Z_y + jZ_{c2}\tan(\frac{\pi f}{2f_0})}{Z_{c2} + jZ_y\tan(\frac{\pi f}{2f_0})}\right) \parallel \left(j2\pi fL_2(1-\frac{f_0^2}{f^2}) + \left(\frac{j2\pi fL_4}{1-\frac{f_0^2}{f^2}} \parallel R_2\right)\right) \tag{48}$$

where

$$Z_y = jZ_{c1}\tan(\frac{\pi f}{2f_0}) \parallel \left(j2\pi fL_1(1-\frac{f_0^2}{f^2}) + \left(\frac{j2\pi fL_3}{1-\frac{f_0^2}{f^2}} \parallel R_1\right)\right). \tag{49}$$

The optimal values of the remaining components are found by solving (46) and (48) numerically for the maximal bandwidth. The results indicate that the L_1, C_1 pair is not needed. For 20 dB and 25 dB cases L_3, C_3 pair is also absent and hence the first isolation network consists of only a resistor, $2R_1$. The normalized component values verified using a microwave circuit simulator are tabulated in Table III. The performance of this divider is depicted in Fig. 13. Its bandwidth is considerably better than that of a two-section Wilkinson divider.

References

[1] E. Wilkinson, "An N-way hybrid power divider," *IEEE Trans. Microw. Theory Tech.*, vol. MTT-8, no. 1, pp. 116–118, Jan. 1960.

[2] S. Cohn, "A class of broadband three-port TEM-mode hybrids," *IEEE Trans. Microw. Theory Tech.*, vol. MTT-19, no. 2, pp. 110–116, Feb. 1968.

[3] R. Ekinge, "A new method of synthesizing matched broad-band TEM-mode three-ports," *IEEE Trans. Microw. Theory Tech.*, vol. MTT-19, no. 1, pp. 81–88, Jan. 1971.

[4] H. Oraizi and A.-R. Sharifi, "Design and optimization of broadband asymmetrical multisection Wilkinson power divider," *IEEE Trans. Microw. Theory Tech.*, vol. 54, no. 5, pp. 2220–2231, May 2006.

[5] N. Ehsan, K. Vanhille, S. Rondineau, E. Cullens, and Z. Popovic, "Broadband micro-coaxial Wilkinson dividers," *IEEE Trans. Microw. Theory Tech.*, vol. 57, no. 11, pp. 2783–2789, Nov. 2009.

[6] J.-C. Chieh and A.-V. Pham, "Development of a broadband Wilkinson power combiner on liquid crystal polymer," in *Proc. Asia Pacific Microw. Conf.*, Dec. 2009, pp. 2068–2071.

[7] J.-S. Lim, U.-H. Park, S. Oh, J. J. Koo, Y.-C. Jeong, and D. Ahn, "A 800 to 3200-mhz wideband cpw balun using multistage Wilkinson structure," in *Proc. IEEE MTT-S Int. Microw. Symp. Dig.*, Jun. 2006, pp. 1141–1144.
[8] S. Wong and L. Zhu, "Ultra-wideband power dividers with good isolation and improved sharp roll-off skirt," *IET Microw. Antennas Propag.*, vol. 3, no. 8, pp. 1157–1163, Dec. 2009.
[9] P. Goodman, "A wideband stripline matched power divider," in *Proc. G-MTT Int. Microwave Symp.*, May 1968, pp. 16–20.
[10] C. T. Chiang and B.-K. Chaung, "Ultra wideband power divider using tapered line," *Progress In Electromagnetics Res*, vol. 106, pp. 61–73, 2010.
[11] K. Hettak, G. Morin, and M. Stubbs, "Compact mmic cpw and asymmetric cps branch-line couplers and Wilkinson dividers using shunt and series stub loading," *IEEE Trans. Microw. Theory Tech.*, vol. 53, no. 5, pp. 1624–1635, May 2005.
[12] R. Mirzavand, M. Honari, A. Abdipour, and G. Moradi, "Compact microstrip Wilkinson power dividers with harmonic suppression and arbitrary power division ratios," *IEEE Trans. Microw. Theory Tech.*, vol. 61, no. 1, pp. 61–68, Jan. 2013.
[13] Y.-S. Lin and J.-H. Lee, "Miniature ultra-wideband power divider using bridged t-coils," *IEEE Microw. Compon. Lett.*, vol. 22, no. 8, pp. 391–393, Aug. 2012.
[14] X. Wang, I. Sakagami, A. Mase, and M. Ichimura, "Wilkinson power divider with complex isolation component and its miniaturization," *IEEE Trans. Microw. Theory Tech.*, vol. 62, no. 3, pp. 422–430, Mar. 2014.
[15] T. Kawai, J. Yamasaki, Y. Kokubo, and I. Ohta, "A design method of dual-frequency Wilkinson power divider," in *Proc. Asia Pacific Microw. Conf.*, 2006, pp. 913–916.
[16] X. Wang and I. Sakagami, "Generalized dual-frequency Wilkinson power dividers with a series/parallel RLC circuit," in *Proc. IEEE MTT-S Int. Microw. Symp. Dig.*, Jun. 2011, pp. 1–4.
[17] Y. Wu, Y. Liu, and S. Li, "Unequal dual-frequency Wilkinson power divider including series resistor-inductor-capacitor isolation structure," *IET Microw. Antennas Propag.*, vol. 3, no. 7, pp. 1079–1085, 2009.
[18] Y. Wu, Y. Liu, and Q. Xue, "An analytical approach for a novel coupled-line dual-band Wilkinson power divider," *IEEE Trans. Microw. Theory Tech.*, vol. 59, no. 2, pp. 286–294, Feb. 2011.
[19] Y. Wu, Y. Liu, Y. Zhang, J. Gao, and H. Zhou, "A dual band unequal Wilkinson power divider without reactive components," *IEEE Trans. Microw. Theory Tech.*, vol. 57, no. 1, pp. 216–222, Jan. 2009.
[20] A. Genc and R. Baktur, "Dual-and triple-band Wilkinson power dividers based on composite right-and left-handed transmission lines," *IEEE Trans. Compon. Packag. Manuf. Technol.*, vol. 1, no. 3, pp. 327–334, Mar. 2011.
[21] J.-C. Kao, Z.-M. Tsai, K.-Y. Lin, and H. Wang, "A modified Wilkinson power divider with isolation bandwidth improvement," *IEEE Trans. Microw. Theory Tech.*, vol. 60, no. 9, pp. 2768–2780, Sep. 2012.
[22] S.-F. Chao and Y.-R Li, "Miniature filtering power divider with increased isolation bandwidth," *Electron. Lett.*, vol. 50, no. 8, pp. 608–610, Apr. 2014.
[23] V. Tas and A. Atalar, "A performance enhanced power divider structure," in *IEEE MTT-S Int. Microw. Symp. Dig.*, 2014, pp. 1–4.
[24] D. M. Pozar, *Microwave Engineering*. New York, NY, USA: Wiley, 1998.
[25] S. Horst, R. Bairavasubramanian, M. Tentzeris, and J. Papapolymerou, "Modified Wilkinson power dividers for millimeter-wave integrated circuits," *IEEE Trans. Microw. Theory Tech.*, vol. 55, no. 11, pp. 2439–2446, Nov. 2007.
[26] C. Trantanella, "A novel power divider with enhanced physical and electrical port isolation," in *IEEE MTT-S Int. Microw. Symp. Dig.*, May 2010, pp. 129–132.
[27] X. Lan, P. Chang-Chien, F. Fong, D. Eaves, X. Zeng, and M. Kinits, "Ultra-wideband power divider using multi-wafer packaging technology," *IEEE Microw. Compon. Lett.*, vol. 21, no. 1, pp. 46–48, Jan. 2011.
[28] S.-H. Kim, J.-H. Yoon, Y. Kim, and Y.-C. Yoon, "A modified Wilkinson divider using zero-degree phase shifting composite right/left-handed transmission line," in *IEEE MTT-S Int. Microw. Symp. Dig.*, 2010, pp. 1556–1559.
[29] X. wang, I. Sakagami, A. Mase, and M. Ichimura, "Trantanella Wilkinson power divider with additional transmission lines for simple layout," *IET Microw. Antennas Propag.*, vol. 8, no. 9, pp. 666–672, Jun. 2014.
[30] H. R. Ahn and S. Nam, "3-dB power dividers with equal complex termination impedances and design methods for controlling isolation circuits," *IEEE Trans. Microw. Theory Tech.*, vol. 61, no. 11, pp. 3872–3883, Nov. 2013.
[31] S. B. Cohn, "Optimum design of stepped transmission-line transformers," *IRE Trans. Microw. Theory Tech.*, vol. MTT-3, no. 3, pp. 16–20, Apr. 1955.

Vahdettin Tas (S'14) received the B.S. degree from Middle East Technical University, Ankara, Turkey, in 2007 and the M.S. degree from Bilkent University, Ankara, Turkey, in 2009, both in electrical engineering, where he is currently pursuing the Ph.D. degree.

In 2009, he was with the Electrical Engineering and Computer Science Department, University of California, Berkeley, CA, USA, as a Research Assistant. From 2010 to 2011, he was an RF Design Engineer at Meteksan Defense, Inc. Since 2011, he has been with the Power Amplifier Technologies Divison, Aselsan, Inc. His current research interests include broadband and efficient power amplification, power coupling, and power combining techniques.

Abdullah Atalar (M'88–SM'90–F'07) received the B.S. degree from Middle East Technical University, Ankara, Turkey, in 1974, and the M.S. and Ph.D. degrees from Stanford University, Stanford, CA, USA, in 1976 and 1978, respectively, all in electrical engineering.

He was with Hewlett Packard Labs, Palo Alto, CA, USA, in 1979. From 1980 to 1986, he was on the faculty of the Middle East Technical University as an Assistant Professor. In 1986, he joined the Bilkent University as the chairman of the Electrical and Electronics Engineering Department and served in the founding of the Department where he is currently a Professor. In 1995, he was a Visiting Professor of Stanford University. From 1996 to 2010, he was the Provost of Bilkent University. He is currently the Rector of the same university. His current research interests include micromachined devices and microwave electronics. He was awarded the Science Award of TUBITAK in 1994.